HHS Public Access

Author manuscript

Nat Genet. Author manuscript; available in PMC 2020 January 29.

Published in final edited form as:

Nat Genet. 2019 August ; 51(8): 1233–1243. doi:10.1038/s41588-019-0470-3.

CELA2A mutations predispose to early-onset atherosclerosis and metabolic syndrome and affect plasma insulin and platelet activation

Fatemehsadat Esteghamat[1], **James S. Broughton**[1], **Emily Smith**[1], **Rebecca Cardone**[1], **Tarun Tyagi**[1], **Mateus Guerra**[1], **András Szabó**[2], **Nelson Ugwu**[1], **Mitra V. Mani**[1], **Bani Azari**[1], **Gerald Kayingo**[1], **Sunny Chung**[1], **Mohsen Fathzadeh**[1], **Ephraim Weiss**[3], **Jeffrey Bender**[1], **Shrikant Mane**[4], **Richard P. Lifton**[5], **Adebowale Adeniran**[6], **Michael H. Nathanson**[1], **Fred S. Gorelick**[1], **John Hwa**[1], **Miklós Sahin-Tóth**[2], **Renata Belfort-DeAguiar**[1], **Richard G. Kibbey**[1], **Arya Mani**[1,4,*]

[1]Department of Internal Medicine, Yale School of Medicine, New Haven, CT, USA.

[2]Center for Exocrine Disorders, Department of Molecular and Cell Biology, Boston University Henry M. Goldman School of Dental Medicine, Boston, MA, USA.

[3]Department of Medicine, NYU Medical Center, New York, NY, USA.

[4]Department of Genetics, Yale School of Medicine, New Haven, CT, USA.

[5]Laboratory of Human Genetics and Genomics, The Rockefeller University, New York, NY, USA.

[6]Department of Pathology, Yale School of Medicine, New Haven, CT, USA.

Abstract

Factors that underlie the clustering of metabolic syndrome traits are not fully known. We performed whole exome sequence analysis in kindreds with extreme phenotypes of early-onset atherosclerosis and metabolic syndrome and identified novel loss-of-function mutations in the gene encoding the pancreatic elastase CELA2A. We further show that CELA2A is a circulating enzyme that reduces platelet hyperactivation, triggers both insulin secretion and degradation, and increases insulin sensitivity. CELA2A plasma levels rise postprandially and parallel insulin levels in humans. Loss of these functions by the mutant proteins provides insight into disease mechanisms and suggests that CELA2A could be an attractive therapeutic target.

* arya.mani@yale.edu.

Author Contributions

F.E. contributed primarily to designing and performing experiments, and preparing the figures and manuscript. J.S.B., R.C., T.T., A.S., N.U., M.V.M., M.G., B.A., S.C., M.F., and A.A. were involved in performing the experiments. S.M., R.P.L., M.H.N., J.H., M.S.-T., and R.G.K. were involved in design and supervision of certain aspects of the project. G.K., E.W., J.B., and E.S. were involved in patient recruitment and clinical characterizations. R.B.-D. carried out all OGTT and hyperglycemic clamp studies. N.U. was involved in the analysis of the genetic data. F.S.G. was involved in design and supervision of aspects of the project and participated in manuscript writing. A.M. designed the study and oversaw its implementation, supervised all aspects of the project from performing the experiments to the analysis of all data, and wrote the manuscript.

Competing Interests

The authors declare no competing interests.

Editorial summary:

Exome sequencing identifies loss-of-function *CELA2A* mutations in families with early-onset atherosclerosis and metabolic syndrome. Functional studies show that CELA2A is a circulating enzyme that reduces platelet activation, triggers insulin secretion and degradation, and increases insulin sensitivity.

Metabolic syndrome is a cluster of inherited risk factors for coronary artery disease (CAD)[1–3], which in outlier kindreds with early-onset CAD may be caused by single gene mutations[4–6]. In this study, we present a cohort of 30 North European index cases with early onset CAD and metabolic syndrome. Combined linkage and gene burden analyses led to identification of multiple independent mutations in *CELA2A*, which encodes the Chymotrypsin-like elastase family member 2A.

CELA2A was primarily known as an “exocrine” pancreatic elastase that preferentially cleaves A-acetyl-L-alanyl-L-alanyl-L-alanine/proline methyl-ester[7] and forms an SDS-resistant complex with alpha-1-antitrypsin (A1AT)[8]. The physiological function of CELA2A outside the exocrine pancreas was not known. Here we characterize the CELA2A protein *in vitro* and *in vivo* and explore the effects of human mutations on its diverse metabolic functions. Using systems biology, we discovered that CELA2A is a circulating protein that impacts diverse biological processes, including insulin secretion, degradation and sensitivity. Our analyses show that impaired regulation of plasma insulin is a major consequence of disease-inducing *CELA2A* mutations. The potential to exploit disease pathways makes CELA2A an appealing target for treating diabetes and its complications.

Results

Clinical characterization of individuals and families with early-onset CAD and metabolic syndrome.

We recruited 30 index cases with early-onset CAD (age of onset at or before 30 y in men and 35 y in women), and extended their kindreds. This led to the identification and recruitment of a multiplex kindred with 25 affected individuals that we named CAD-2001 (Fig. 1a). The index case was an American female of European ancestry with extensive family history of CAD, and first ST elevation myocardial infarction (STEMI) at age 28 y (arrow). Her CAD risk factors included hypertension (HTN), type 2 diabetes (T2D), hypertriglyceridemia (HTG), and obesity. She underwent a coronary artery angiography and percutaneous intervention of two major coronary arteries. Among 53 extended blood relatives of the index case, 25 were diagnosed with early onset CAD (MI diagnosis by enzyme and EKG, angiographic diagnosis of CAD, or sudden cardiac death) with median age of 43 y, and 11 had died from CAD (mean age of death of 52 y). All affected individuals traced their ancestry to a common ancestor, and male-to-female transmission of the phenotype was present.

Detailed clinical data were available for all 11 living family members with CAD, two younger family members (mean age 30 y) with unknown CAD status, and 12 living unaffected family members (Supplementary Table 1). All affected individuals met the NCEP

criteria for metabolic syndrome with surprisingly homogeneous risk factors, including markedly elevated triglycerides (TG) (mean 287.1 mg/dl, Nl < 150 mg/dl), hypertension, low HDL (mean 35.1 mg/dl, Nl > 50 mg/dl) and T2D (fasting blood glucose > 126 mg/dl or on glucose lowering drugs). In contrast, all 12 unaffected family members had normal TG (mean 100.5 mg/dl) and near normal HDL levels, and none had T2D. The two younger family members with unknown CAD status had both HTG and HTN. The familial clustering and pattern of inheritance of these clinical features were consistent with the effect of a highly penetrant autosomal dominant trait.

Whole exome sequencing identifies mutations in *CELA2A* underlying CAD.

We carried out a gene burden analysis using whole exome data of all 30 index cases. An independent genetic analysis was carried out in the CAD-2001 pedigree (Fig. 1a), using 35 DNA samples of the affected and unaffected family members. The unbiased analysis of whole exome sequence data from affected family members of CAD-2001 with angiographically diagnosed CAD led to identification of a single shared 4.8-Mb chromosomal interval (11,102,837–15,933,568) on chromosome 1, flanked by two SNPs rs225874 and rs848210 (Fig. 1b). Within the linked interval, we identified a single non-conservative missense mutation (1:15789885 G>A, hg19) in exon 6 of *CELA2A*. The mutation results in substitution of the evolutionarily highly conserved and functionally indispensable aspartic acid of the catalytic domain at codon 121 for asparagine (p.D121N) and perfectly segregates with CAD in all 12 affected family members. No other non-conservative segregating mutation was identified, and the presence of a shared structural variant was excluded by whole genome sequencing in two remotely related affected individuals (II-10 and IV-2). The p.D121N amino acid substitution was predicted to be damaging by PolyPhen-2 (score of 1.000) and SIFT (score of 0) assessments[9]. A two-point linkage analysis revealed a LOD score of 6.9 (odds ratio 7,758,879:1 in favor of linkage) between CAD and the *CELA2A* locus. The individuals with HTG and HTN and unknown CAD status were also carriers of p.D121N. Hence, we considered the impact of this mutation on CAD risk factors. The linkage between the *CELA2A* locus and HTN was stronger compared to CAD (LOD = 7.48) (Supplementary Table 2). The difference in mean TG levels between mutation carriers and non-carriers was also significant (Supplementary Table 3). Because HTN and HTG are found in most mutation carriers (Supplementary Table 1 and Supplementary Fig. 1a), these traits could serve as biomarkers of the mutation in individuals too young to manifest CAD. Similarly, p.D121N was associated with BMI (Supplementary Fig. 1b) and T2D (Supplementary Table 3). There was lower plasma cortisol levels in mutation carriers vs. non-carriers, while plasma GLP1 and globular adiponectin levels were not significantly different (Supplementary Fig. 1c–e).

Strikingly, the analysis of whole exome sequencing in all 30 index cases showed the highest burden of novel nonconservative mutations in *CELA2A* gene. Two *CELA2A* missense and one splice site mutations were identified in 3 unrelated index cases. All mutations were novel and non-conservative, and the missense mutations were predicted to be deleterious by SIFT and PolyPhen-2. No other gene was identified with more than two mutations in all 30 exomes. Only two predicted deleterious *CELA2A* mutations were identified in 4,000 control chromosomes of healthy individuals of European ancestry (Yale control exome database).

Statistical analysis by Mann-Whitney test showed that recurrent mutations in this gene in 30 subjects is unlikely to have occurred by chance ($P < 3.1 \times 10^{-5}$, Monte Carlo simulation).

The mutation 1:15789253 C>A, which results in p.L85M substitution, was found in a female of European ancestry (Fig. 1c) with a strong family history of CAD, who had undergone percutaneous coronary intervention (PCI) to left anterior descending (LAD) at age 34 y, HTG (TG > 234 mg/dl) and low HDL (26 mg/dl). The third mutation was found in a 24-year-old male of European ancestry with CAD and his uncle (Fig. 1d), who had developed CAD in his early 40's. Both individuals and the deceased father of the index case had HTG (TG > 350 mg/dl), HTN, and T2D. This mutation was a single nucleotide substitution 1 bp upstream of the splice site for exon 6 (splice donor c.639+1, 1:15792640 G>C). Based on predictive programs and functional analysis (see below), this mutation leads to an alternative splice site and generates a stop codon 30 bp distal to exon 6, with generation of a truncated protein that lacks the nucleophilic active Ser216. The fourth mutation (1:15788135 C>T) was identified in a woman of European ancestry with CAD at age 30 y (Fig. 1e). This mutation leads to substitution of the highly conserved threonine at codon 70 with methionine (p.T70M). All mutated nucleotides alter evolutionarily highly conserved residues located in or near the catalytic domains (Fig. 1f,g); none were present in the Yale control exome database, and they have allele frequencies between 2×10^{-4} and 2×10^{-5} in the gnomAD database. Most importantly, no amino acid substitutions were found for any of the three amino acids in the catalytic domain in Yale exome or ExAC databases ($n = 10{,}000$). These results support the association of novel and deleterious *CELA2A* mutations with CAD and metabolic syndrome.

Interestingly, common intronic *CELA2A* variants rs1042010 and rs3820068 have been associated with elevated systolic blood pressure by independent genome-wide association studies[10–12] ($P < 3 \times 10^{-13}$ and $P < 1 \times 10^{-12}$, respectively). Further analysis revealed that the rs1042010(G) allele is in disequilibrium with the eSNP rs3753326(A) ($D' = 0.8674$, $r^2 = 0.7134$; Chi-sq = 3572.8956; $P < 0.0001$), which is reportedly located in an open chromatin region (http://www.regulomedb.org/snp/chr1/15790973) and is associated with reduced *CELA2A* transcription in the adrenal gland (GTEx database, $P = 2.4 \times 10^{-9}$).

Human *CELA2A* mutations abolish its elastase activity.

Wild-type (WT) and mutant *CELA2A* constructs were expressed in HEK293T cells, and the cell lysate and conditioned media were examined for CELA2A protein expression. Western blot analysis of the conditioned media showed the expected 25-kDa band and a 75-kDa band that was resistant to denaturing conditions prior to loading (Fig. 2a), was found to be enriched in CELA2A and few other proteins by proteomic analysis (Supplementary Table 4), and was absent in p.D121N and p.T70M (lanes 3, 4). Expression of the *CELA2A* construct containing the splice site variant led to the generation of a weak band of somewhat lower molecular weight in cell lysate that was undetectable in the conditioned medium.

We then examined the elastase activities of the wild-type vs. mutant CELA2A proteins. It is notable that D121 constitutes one of the three amino acids of the catalytic triad (Fig. 2b)[13], which forms a low-barrier hydrogen bond between its beta-carboxyl group and N delta 1 of His73, stabilizes the positive charge on its active site, and plays a crucial role in nucleophilic

activity of Ser216[14]. Accordingly, the elastase activity of p.D121N-CELA2A on a synthetic substrate containing the canonical cleavage site[15] was considerably lower than WT-CELA2A (Fig. 2c). Purified p.L85M, p.T70M and splice variant CELA2A proteins also exhibited dramatic reduction in elastase activity. The elastase activities of co-expressed wild-type and mutant CELA2A proteins were significantly less than sum of their individual activities, consistent with a dominant-negative effect of the mutant proteins (Fig. 2d). Western blot analysis of purified A1AT treated with the purified CELA2A proteins showed that, in contrast to wild-type CELA2A[7] (75-kDa band, Fig. 2e, lane 2), p.D121N, p.T70M, and splice-variant CELA2A form no complex and p.L85M-CELA2A forms a small complex with alpha-1-antitrypsin (A1AT) (lane 6).

CELA2A is a circulating protein.

The array of traits associated with the *CELA2A* mutations suggested a systemic effect of the encoded protein and led to examination of its tissue distribution. The specificity of the antibody for western blot analysis was verified by pre-blocking with rCELA2A and testing that on secreted CELA2A from CELA2A-transfected-HEK293T cells or the serum fractions (Supplementary Fig. 2a,b), and for immunohistochemistry by staining mouse skeletal muscle before and after rCela2a injection (Supplementary Fig. 2c). The ELISA kit was validated for cross reactivity between human and mouse using vehicle and different titers of purified human WT- and p.D121N-CELA2A and rCela2a (Supplementary Fig. 2d). In mice, the highest mRNA and protein levels were found in the pancreas (Fig. 3a,b). We further examined its protein expression by immunohistochemistry; strong signals were also observed in the adrenal gland and small intestine (Supplementary Fig. 3a–c). We then examined the expression of CELA2A in human surgical specimens (Fig. 3c). The most intense staining was observed in exocrine pancreas. A small fraction of cells in pancreatic islets also stained positive for CELA2A. In addition, adrenal cortex, intestinal glands and colonic lymphoid follicles stained positive for CELA2A. CELA2A of human cadaveric pancreas, liver and white adipose tissue were further verified by western blot analysis (Supplementary Fig. 3d).

Interestingly, data extracted from Gene Expression Omnibus (GEO) show elevated expression of *CELA2A* in disease states in tissues that have otherwise no or low expression levels of CELA2A including skeletal muscle of insulin resistant obese subjects[17] and β cells of subjects with T2D[18] (Supplementary Fig. 4a,b).

We subsequently examined and verified the presence of CELA2A in human plasma. Western blot analysis of human serum with CELA2A antibody recognized 75-kDa and 25-kDa bands that were absent when Cela2a-antibody was preblocked with rCELA2A (Fig. 3d). Plasma CELA2A and glucagon levels were assayed by validated ELISA and were found to be higher in p.D121N- than WT-CELA2A carriers (Fig. 3e and Supplementary Fig. 4c). However, the total plasma elastase activity was reduced by greater than 1.75–fold in mutation carriers compared to non-carriers (Fig. 3f), indicating a substantial contribution of CELA2A to total circulating elastase activity.

Plasma CELA2A levels rise postprandially and parallel plasma insulin levels.

Since T2D was a common trait among mutation carriers, we posited that CELA2A might regulate insulin secretion. We first measured baseline and postprandial plasma CELA2A, insulin and C-peptide levels in healthy controls (mean age 35 y) by ELISA (Fig. 3g–i). The responses to a meal for plasma CELA2A, insulin and C-peptide were virtually identical (R^2 coefficient 0.9 and 0.88, respectively) (Fig. 3j,k), while glucagon levels showed an inverse relationship with plasma CELA2A (Supplementary Fig. 4d,e; R^2 coefficient −0.72). The parallel surge of CELA2A and insulin and raised the possibility that CELA2A acts as an insulinotropic peptide.

We subsequently compared the effect of oral vs. intravenous glucose on plasma CELA2A levels in obese nondiabetic individuals subjected to a hyperglycemic clamp and oral glucose tolerance test (OGTT). A hyperglycemic clamp, designed to keep glucose levels clamped around 200 mg/dl, led to higher plasma insulin and CELA2A levels (Fig. 3l). The OGTT of the same individuals showed a parallel rise of plasma CELA2A and insulin (Fig. 3m). The plasma CELA2A to glucose ratios at 60 min were similar between OGTT and hyperglycemic clamp studies (Supplementary Fig. 4f). There was an inverse relationship between plasma CELA2A and glucagon levels in both studies (Supplementary Fig. 4g,h).

CELA2A promotes glucose-induced calcium ion dependent insulin secretion.

To explore the *in vivo* effect of CELA2A on glucose and triglyceride homeostasis, three-month-old male hyperlipidemic and diabetic $Ldlr^{-/-}$ mice on Western diet were injected intravenously with exogenous endotoxin-free (<0.1 EU/ml, Gene Script, L00338) mouse rCela2a (2.5 mg/kg) ($n = 10$) or vehicle ($n = 10$) after 16 h fasting. Mice injected with saline maintained normal glucose levels, while mice injected with rCela2a exhibited continuous fall in plasma glucose (Fig. 4a). Circulating levels of C-peptide and insulin to glucose ratios were strikingly higher in rCela2a treated mice (Fig. 4b,c). These findings could be due to enhanced secretion, reduced clearance or degradation of insulin in response to rCela2a administration, or combination thereof. No significant change in plasma TG was noted (data not shown). Interestingly, rCela2a did not induce insulin secretion in normoglycemic C57BL/6 mice (Supplementary Fig. 5a,b), indicating a glucose-dependent function.

To investigate the direct effect of rCela2a on insulin secretion, size-matched primary rat islets were treated with rCela2a (2.8 μg/ml) or a vehicle at 2.5 mM and 9 mM glucose concentrations; KCl (KCl30, Fig. 4d) administration was used as a test for islet viability. Insulin secretion was augmented by rCela2a at 9 mM glucose compared to vehicle alone (Fig. 4d). Human islets treated with WT-CELA2A showed significantly higher C-peptide and tendency toward higher insulin secretion compared to controls (Supplementary Fig. 5c,d). It is noteworthy that WT-CELA2A purified in the laboratory had a weaker effect on human islets than rCela2a (Supplementary Fig. 5e).

Voltage-gated L-type calcium channels (Cav1.1–1.3) mediate beta-cell insulin secretion. Cav1.1 and Cav1.2 have been shown to undergo proteolytic cleavage in their highly conserved distal C-terminal domain and form a complex with the truncated α_1-subunit and PKA[19,20], leading to their activation. Proteomics/phosphoproteomics analysis of INS-1 cells

treated with rCela2a exhibited detectable activation of PKA and higher levels of CACNA1A and CACNA1D phosphorylation compared to the vehicle alone or untreated cells (Supplementary Table 5). Accordingly, intracellular Ca^{2+} transient was dramatically increased after rCela2a treatment of INS-1 cells in the presence of 9 mM glucose compared to vehicle (Fig. 4e).

In addition, there was upregulation of proteins involved in vesicle transport and insulin secretion. Accordingly, gene enrichment analysis of proteins/phosphoproteins increased by >1.5-fold after rCela2a treatment (adjusted $P \leq 0.01$) identified the "Regulation of Insulin Signaling" as one of the three top ranked gene sets (Supplementary Table 6).

Impaired insulin degradation and sensitivity of mutant CELA2A proteins.

We compared the effect of WT-CELA2A vs. p.D121N-CELA2A on insulin secretion in rat islets. Rat islets treated with WT-CELA2A showed only a trend toward higher secretion of insulin but significantly higher C-peptide secretion at the 9 mM glucose concentration compared to p.D121N-CELA2A (Fig. 5a,b, second phase). Accordingly, WT-CELA2A triggered greater intracellular Ca^{2+} transients in INS-1 cells compared to p.D121N-CELA2A at 9 mM glucose (Fig. 5c,d). These findings indicated that p.D121N substitution impairs the activity of CELA2A in augmenting glucose-dependent calcium receptor activation and insulin secretion. However, the absence of substantial difference in insulin as opposed to C-peptide secretion between WT-CELA2A and p.D121N-CELA2A raised the possibility that CELA2A proteolytically degrades insulin and loss of this functions by p.D121N-CELA2A may contribute to the elevated insulin levels observed in nondiabetic CELA2A mutation carriers (IV-2 and IV-3 in the D121N kindred had documented fasting insulin levels of 142 and 79.5 mg/dl, respectively). Insulin secretion and degradation has been shown for insulin degrading enzymes[23,24] and some pancreatic proteases[25]. Thus, we measured intact insulin levels in rat islets treated with WT- and p.D121N-CELA2A for 48 h in the presence of 9 mM glucose. Strikingly, after 48 h there were lower insulin levels in the medium of rat islets treated with WT- vs. p.D121N-CELA2A (Fig. 5e). We verified the effect of purified wild-type and different mutant CELA2A proteins on insulin degradation using Ultra Performance Liquid Chromatography (UPLC). The analysis showed that wild-type but not mutant CELA2A proteins (with the exception of p.L85M) cause insulin fragmentation (Fig. 5f).

It has been shown that loss of insulin degrading peptide CEACAM1 causes hyperinsulinemia and triggers insulin resistance[26]. We therefore examined the effect of WT- and p.D121N-CELA2A (300 pg/ml) on insulin-signaling pathway in 3T3L1 cells after 24 h starvation at 0, 15, 30 and 45 min. Western blot analysis showed that WT-CELA2A but not p.D121N-CELA2A enhances insulin signaling activity after 15 min (Fig. 5g, quantification in Supplementary Fig. 6a–e). Insulin pre-incubated with WT-CELA2A showed lower signaling activity compared to insulin alone and insulin pre-incubated with p.D121N-CELA2A, consistent with its proteolytic degradation by WT-CELA2A.

CELA2A inhibits platelet activation.

In screening for proteins with extracellular CELA2A target site(s)[15], we came across integrin A2B, which binds integrin beta-3 to generate GPIIb/IIIa receptor complex. Upon

binding of soluble fibrinogen, the receptor complex triggers platelet aggregation/activation. The effect of purified wild-type and mutant CELA2A (300 pg/ml) proteins on human platelet aggregation (n = 4 healthy volunteers, age 30–60 y, with collagen as the agonist) was measured by using Lumi-aggregometer (Chrono-Log). WT-CELA2A reproducibly reduced while p.D121N-CELA2A increased the platelet aggregation as compared to vehicle (Fig. 6a). Platelet aggregation was also visualized by a platelet adhesion assay using confocal microscopy (Fig. 6b). The degree of aggregation and size of platelet aggregates were dramatically increased after treatment with p.D121N-CELA2A compared to WT-CELA2A. We carried out a PAC1 binding assay to examine structural changes in platelet GPIIb/IIIa complex that marks their activation in response to WT- vs. p.D121N-CELA2A[27]. WT-CELA2A reduced while p.D121N-CELA2A increased PAC1 binding compared to vehicle treated platelets (Fig. 6c). The apoptotic tendency of platelets treated with WT- or p.D121N-CELA2A was assayed based on the measurement of mitochondrial inner membrane potential ($\Delta\Psi m$) using tetramethylrhodamine ethyl ester dye (TMRE)[28]. TMRE-negative cells were reduced by WT-CELA2A treatment by about 3.5–5% and increased by p.D121N-CELA2A between 3–5% (Fig. 6d), suggesting enhanced platelet apoptosis by the mutation.

Treatment of purified GPIIb/IIIa integrin by WT-CELA2A but not p.D121N-CELA2A resulted in cleavage of ITGA2B component and generation of a smaller 75-kDa band (Fig. 6e). The mass spectrometry-based analysis of the 75-kDa band showed that it is composed of CELA2A and ITGA2B fragments, further confirmed by western blot analysis (Fig. 6f). Platelet aggregation was also increased by p.T70M- and p.L85M-CELA2A proteins (Fig. 6g). Together, these findings suggest that WT-CELA2A binds to and cleaves ITGA2B, thus limiting activation of platelets. In contrast, mutant CELA2A promotes hyperactivation and aggregation of platelets.

Discussion

Our study establishes an association between mutations in *CELA2A* gene and early-onset CAD and metabolic syndrome. Our success in identifying single gene mutations underlying CAD and metabolic traits is the result of a unique approach to ascertain kindreds with clustering of extreme phenotypes, including early age of onset of CAD and HTG. The evidence for disease causality of *CELA2A* variants includes identification of multiple independent non-conservative mutations in disease subjects, perfect disease segregation of a novel loss-of-function mutation in a large multiplex kindred, unraveling the disease relevant functions of the protein, and strong biochemical data indicating loss of function of the mutant proteins.

Most carriers of the *CELA2A* mutations had early onset CAD, HTG, HTN and T2D, and met the criteria for the metabolic syndrome. These observations indicate the broad and important effect of *CELA2A* mutations and suggest that the clustering of the individual risk factors imparts extremely high cardiovascular risk to mutation carriers. Very little is known about the function of CELA2A and its role in human disease. The demonstration of CELA2A as a circulating protein in human and mouse, its expression in diverse tissues and the reduced plasma elastase activity in mutation carriers vs. non-carriers are all indicative of its important systemic effects.

We elucidated two functions of CELA2A that potentially relate to the phenotype of mutation carriers (Fig. 7): regulation of plasma insulin and restraining platelet activation. The most striking function of CELA2A disclosed by our study was its role in regulating glucose-dependent insulin secretion and degradation. Strikingly, Cela2a triggered insulin secretion and hypoglycemia in hyperglycemic $Ldlr^{-/-}$ mice, but caused hyperglycemia and low plasma insulin levels in normoglycemic mice, likely due to insulin degradation in the absence of excess secretion. The postprandial rise of CELA2A and strong correlation with plasma insulin and C-peptide levels in healthy human controls and in obese nondiabetic subjects undergoing OGTT and clamp studies confirmed a near perfect correlation between plasma CELA2A and insulin levels and suggested an insulinotropic effect of CELA2A. The *in vitro* effects of CELA2A in mouse and human islets are less strong and have shorter durations than its *in vivo* effects; this difference could potentially be due to unknown circulating modifiers that modulate its function in intact animals.

The insulin degradation by CELA2A appears to be the most compromised function by the p.D121N substitution as evidenced by severe hyperinsulinemia of the nondiabetic mutation carriers. Whether chronic hyperinsulinemia causes beta-cell dysfunction is not certain but has been described in *Ceacam1* knockout mice[26] and streptozocin-induced neonatal diabetic rats (NSZ rats) prior to developing of beta cell defect[30].

Finally, our findings suggest that CELA2A enhances insulin signaling and may have physiological role in cellular glucose metabolism. These functions are very similar to those of the insulin degrading enzyme (IDE)[23,24] and CEACAM1[26] and are impaired by p.D121N substitution.

Our analysis showed that p.D121N carriers have reduced elastase activities but higher total CELA2A protein levels compared to non-carrier relatives. Whether the catalytic inactive p.D121N-CELA2A has certain gain-of-function effects is unclear at this point. Interestingly, individuals with T2D appear to have higher GLP-1 levels[31] but are more resistant to it compared to normal subjects[32]. Future studies in individuals with T2D should be directed at determining CELA2A levels, its biological half life time, and its effect size.

Our results indicated that WT-CELA2A proteolytically degrades GPIIb/IIIa and reduces platelet aggregation. This is in contrast to the proteolytic degradation of GPIIb/IIIa by chymotrypsin, which results in generation of different fragments and enhanced platelet aggregation[33]. This function, which is impaired by *CELA2A* mutations, extends the potential therapeutic application of this protein.

Elastases target different components of the extracellular matrix (ECM)[34] and may facilitate the regeneration of elastin fibers in the aorta[35]. Association between decreased serum elastase activity, increased serum elastase inhibitor activity and increased accumulation of carotid plaque has been shown in longitudinal human studies[36]. These findings differ from those related to neutrophil elastases and their putative roles in atherogenesis[37] and insulin resistance[38] and may be attributed to the structural and biological differences between distinct elastases, their tissue-specific activities or the relatively narrow range of their physiological concentrations.

In conclusion, our genetic studies associate mutations in *CELA2A* with a clinical phenotype that is characterized by early-onset CAD, and metabolic syndrome. In addition, our *in vivo* and *in vitro* studies identify CELA2A as a peptide with systemic functions and as a potential candidate for developing novel therapeutics for treating atherosclerosis, thrombosis and impaired glucose tolerance.

Methods

Ascertainment and recruitment of cases.

The study protocol was approved by the institutional review board of Yale University, and written informed consent was obtained from all study participants. The index cases had been identified as individuals with early onset CAD, defined as first time angiographic diagnosis of CAD at or before age 30 y in men and 35 y in women with only modest hyperlipidemia and without familial hypercholesterolemia. All available family members of the index cases willing to participate in the study were recruited and their medical records were reviewed. The kindreds examined are of European ancestry, with all members living in the United States. Venous blood samples were obtained from all index cases and members of their extended kindred and were used for DNA extraction, routine blood chemistry, plasma lipids and metabolomics. Participants were considered hypertensive if they had blood pressures greater than 140/90 mmHg or were receiving antihypertensive medications, and were considered diabetic or to have impaired glucose tolerance if they were taking glucose lowering mediations or had a fasting blood sugar greater than 126 mg/dL or 100 mg/dl, respectively. Participants were considered overweight if they had a BMI > 25 kg/m^2 and obese if they had BMI > 30 kg/m^2. Plasma lipids were considered as continuous variables.

Whole exome and whole genome sequencing.

Exome data for 30 index cases and the extended family members with the diagnosis of early-onset CAD and metabolic syndrome, and the Yale control exome database were all generated at the W. M. Keck Facility of Yale University, as described[6]. The Roche/Nimble-Gen 2.1M Human Exome Array covers 34.0 Mb of genomic sequence and about 180,000 exons of 18,673 protein-coding genes. Briefly, extracted DNA was fragmented, ligated to linkers and fractionated by agarose gel electrophoresis. Extracted DNA was amplified by PCR and hybridized to the capture arrays. Resulting bound DNA was eluted, purified and amplified by ligation-mediated PCR. The PCR products were purified and sequenced on the Illumina DNA sequencing platform. Captured data was analyzed on the Illumina genome analyzer, followed by Image analysis and base calling. The resulting sequences were mapped to reference genome hg19 and processed using Maq software. SAMtools software was used to detect single nucleotide variants (SNVs). The SNVs were then filtered out as described[39]. Filters were applied against a published database. The frequency, pathogenicity and location of mutations occurring in NHLBI, ExAC database and Yale control databases were examined. Variants were filtered for allele frequencies greater than 0.001% in ExAC database. A Perl-based computer script was used to annotate variants based on protein effect, novelty, conservation and tissue expression. Mutation pathogenicity was assessed using PolyPhen-2 and SIFT predicting software[9] and filtered if considered not damaging by either software.

A two-point parametric analysis of linkage was carried out using data obtained from the members of the largest kindred, specifying coronary artery disease as an autosomal dominant trait. Disease allele frequencies was specified as 10^{-5}, and the phenocopy rates of 10^{-4}.

To assess the prevalence of identified mutations in disease and control populations, exome data from the Yale control, NHLBI and ExAC databases were screened for variants in the *CELA2A* gene. The NHLBI exome database[40], accessed on 20 October 2013, consisted of 6,503 CAD case and control samples from multiple Exome Sequencing Project cohorts. The Yale control exome database included exome data from control population of 2,000 Northern European individuals free of CAD and metabolic conditions.

To exclude structural variation, two DNA samples from independent mutation carriers were subjected to whole genome sequencing. IGV was used to assess copy number variation by using Variant Effect Predictor (VEP) and WGS Annotator (WGSA).

Antibodies, recombinant proteins, and ELISA kits.

Purified GP2B3A complex (MBS135714), mouse rCela2a protein (MBS1246487), human rCELA2A (MBS1090462) and the CELA2A ELISA kit (MBS932150) were purchased from MyBiosource. CELA2A antibody (SAB1104798) and the elastase substrate N-Succinyl-Ala-Ala-Pro-Leu p-nitroanilide substrate (S8511) were purchased from Sigma-Aldrich. The FITC-conjugated PAC1 antibody (340507, BD Biosciences) and tetramethylrhodamine ethyl ester (TMRE) reagent (T669, Thermo Fisher Scientific), Annexin V-FITC (640905, Biolegend), CD41-FITC (303703, Biolegend) were used for platelet aggregation analysis. Total AKT (CST, 9272), pAKT (S473) (CST, 9271s), pAKT (T308) (CST, 9275s), total S6k (CST, 9202), pS6k (T389) (CST, 9206), total IRS (CST, 2382), pIRS (Y608), (CST, 2385S), pIRS (S636/S639) (CST, 2388s), Gapdh (CST, 3683s), and Actin (CST, 4970) antibodies were purchased from Cell Signaling Technologies. Recombinant A1AT (alpha1 antitrypsin, ab91136), A1AT antibody (ab9400) and ITGA2B antibodies (ab63983) were purchased from Abcam. Human c-peptide ELISA kit (80-CPTHU-E01.1, ALPCO), Human Glucagon ELISA kit (10-1271-01, Mercodia), Rat c-peptide ELISA (80-CPTRT-E01, ALPCO), Mouse Ultrasensitive Insulin ELISA (80-INSMSU-E01, ALPCO), Human Insulin ELISA kit (21-IAAHU-E01, ALPCO), Rat Insulin ELISA kit (80-INSRT-E01, ALPCO) was applied for C-peptide, glucagon, and insulin measurements.

Tissue expression of CELA2A.

For QRT-PCR analysis, RNA was extracted using TRI reagent (Sigma-Aldrich) according to the company's protocol. To synthesize cDNA, 2 μg of RNA was used with oligo dT, RNase OUT, SuperScript reverse transcriptase II (Invitrogen) in a total volume of 20 μL, and 0.3 μL of cDNA was used for further amplification by QRT-PCR. Amplification was performed with primers F (5'-CTGGCACCATTCTCCCGAGAAA-3') and R (5'-GTGGCATAGTCCACAACCAGCA-3') using Platinum Taq DNA polymerase (Invitrogen) and 40 cycles consisting of 94 °C for 30 s, 60 °C for 30 s, and 72 °C for 30 s.

Protein expression.

CELA2A protein expression was examined in mouse tissues using western blot analysis. Tissue lysates were prepared from C57BL/6 mice, and protein content was measured in lysates by Bradford assay. Lysate dilutions of equal protein concentration were separated by SDS-PAGE and processed for immunoblot analysis to assess the CELA2A protein level. Immunohistochemistry was used to visualize the CELA2A antigen in mouse tissues; a non-immune rabbit IgG served as a labeling control.

Validation of the CELA2A antibody and the ELISA kit.

Protein levels were assessed by a validated CELA2A-specific antibody (Sigma), with a double band representing the zymogen and active form of the protein. This antibody recognizes both human and mouse CELA2A and its specificity and cross-reactivity were confirmed using recombinant mouse CELA2A (rCela2a) protein, the supernatant collected from the 293T cells overexpressing human CELA2A and by pre-blocking the antibodies with rCela2a protein (Supplementary Fig. 2a,b). The antibody specificity was confirmed by blocking 1 μg of antibody (Sigma, SAB1104798) with 2.5 μg of rCela2a, followed by western blot analysis. To test the specificity of the antibody for immunohistochemistry, skeletal muscle tissue was used as a negative control for CELA2A labeling and non-immune IgG as an antibody control. The skeletal muscle tissue of the C57Bl/6 mice after intravenous injection with the rCela2a protein was used as positive control.

To test the specificity of the ELISA (MyBioSource) for human CELA2A, 1 μl and 2 μl of purified human WT- or p.D121N-CELA2A with a protein concentrations measured previously by Bradford assay were assayed for concentration by ELISA (Supplementary Fig. 2d). The consistency between ELISA and Bradford measurements was confirmed.

Serum fractionation.

200 μL of mouse serum was separated by size exclusion chromatography on a 1.5 cm × 31.5 cm column comprised of Sepharose 6b beads (fractionation range: 10 kDa to 1,000 kDa). The column buffer was 5 mM HEPES + 50 mM NaCl + 0.1 mM $CaCl_2$ at a pH of 7.4; 450 μl fractions were collected. Fraction number 65 was used for CELA2A detection (bands observed at 25 kDa and 75 kDa).

Human plasma CELA2A measurement and associated elastase activity assay.

CELA2A plasma levels were measured by ELISA. Briefly, 50 μl of plasma was incubated with CELA2A-antibody coated 96-well plated provided by the kit for 1 hour at 37 °C, washed x3, then incubated with the HRP-conjugated secondary antibody for 1 h. After color development, absorbance was measured at 450 nm and compared to a standard curve.

Plasma elastase activities of family members were assessed by first diluting sample 1:5 in 0.2 M Tris/HCl buffer containing 0.2 M NaCl with 10 mM $MgCl_2$ and 10 mM $CaCl_2$. Succinyl-trialanyl-nitroanilide was used as the substrate; it was dissolved in 0.92% (v/v) N-methyl-pyrolidone at 12.5 mM. 100 μL of substrate solution was added to 7 μL of diluted samples and incubated for 1 h, at which time the assays were stopped by adding 50 μl glacial

acetic acid, and absorbance were measured at 410 nm. Purified porcine pancreatic elastase was used to generate a standard curve.

Generation and purification of wild-type and mutant CELA2A.

cDNA generation and site directed mutagenesis and insertion of the wild-type and mutant constructs in pcDNA3.1-*CELA2A*-His plasmids were carried out per routine. Briefly, HEK293T cells were seeded in a 6-well plate using DMEM, 10% FBS, and antibiotics. Cells were transfected 24 h later with the plasmids, 10 μL Lipofectamine 2000 and rinsed 48 h later and covered with 2 mL OptiMEM. All transfections were performed in duplicates. 50 μL of the collected conditioned media was loaded on a 4–15% gradient SDS-polyacrylamide gel and visualized by Coomassie Brilliant Blue staining.

CELA2A purification was carried out as described[41]. Briefly, the wild-type and mutant CELA2A constructs with a His-tagged at the C-terminus were generated and inserted in a pcDNA3.1 vectors, under CMV promoter and expressed in HEK293T cells. HEK293T cells were cultured in Dulbecco's Modified Eagle Medium (DMEM, Thermo Fisher Scientific) with 10% fetal bovine serum (FBS, Thermo Fisher Scientific), supplemented with 4 mM L-glutamine at 37 °C, in 5% CO_2 to about 80–90% confluence. Subsequently, cells were transfected with plasmid DNA and incubated for 16–20 h and subsequently washed and covered with Opti-MEM medium (Thermo Fisher Scientific). After 48 h incubation, the conditioned media were extracted and purified using Ni-affinity chromatography on a 1 mL Ni-NTA Superflow Cartridge (#30210, Qiagen). The column was equilibrated and 720 CC medium was loaded. After the column was washed with the NPI-20 buffer and zymogens were eluted with buffer NPI-250 (50 mM NaH_2PO_4, 300 mM NaCl, 250 mM imidazole (pH 8.0) and 1 mL fractions were collected. The aliquots of the fractions were analyzed by SDS-PAGE for zymogen concentration and those with the highest concentrations were pooled and dialyzed, and concentrated to a volume of 1–3 mL by centrifugation. Concentrations of purified CELA2A solutions were estimated using ultraviolet (UV) absorbance at 280 nm and confirmed by ELISA assay.

Elastase activity, proteolytic cleavage of A1AT, GP2B3A, and insulin by wild-type and mutant CELA2A.

To measure elastase activities, wild-type and mutant CELA2A propeptides were activated with 7 μL of 6 μM human anionic trypsin together with 2 μL Tween 20, 40 μL 1M Tris-HCl (pH 8.0) and 4 μL of 1 M $CaCl_2$, added to 400 μL conditioned medium and incubated at 37 °C for 30 min. Next, 185 μL wild-type or mutant CELA2A were added to 15 μL of 6 mM Suc-Ala-Ala-Pro-Leu-pNA substrate. The reaction was analyzed on a 405 nm in plate reader. Assays were carried out in triplicate, and mean ± s.e.m. are shown. For expression studies, HEK293T cells were transfected with 4 μg WT-His-CELA2A or 2 μg WT-CELA2A and 2 μg mutant-His-CELA2A constructs. Conditioned media was used to measure the elastase activity followed by the aforementioned protocol.

0.5 μg of activated purified wild-type or mutant CELA2A were incubated with 2 μg A1AT or 2 μg GPIIB/IIIA for 16 h. Samples loaded on 4–15% gradient SDS gel, blots were incubated with antibodies against A1AT or ITGA2B and developed afterwards. 0.5 μg of

activated purified wild-type and mutant CELA2A were incubated with 1 μg Insulin Chain B Oxidized from bovine pancreas (I6383–5MG) and samples were subjected to the UPLC analysis.

Analysis of insulin fragmentation by ultra-performance liquid chromatography (UPLC).

The spectral analysis of digested recombinant insulin fractions was carried out using AcQuity H Class system with a PDA fraction collector. XBridge Protein BEH C4, 300A, 1.7 μm, 2.1×150 mm column was used for UPLC separation with temperature set as 40 °C. Distilled water supplemented with 0.1 % TFA was used as mobile phase A, and 71.4 % acetonitrile and 0.075 %TFA as B. The flow rate was 0.2 ml/min. Initial condition was set as 28%, maintained for 1 min, and then ramped up to 100 % in 25 min, maintained for 4 min and back to initial condition in 1 min and equilibrated for 9 min before next injection. Fraction collector was set as 0.2 min collection per vial.

Insulin secretion in rat islets.

Intact islets isolated from ~300–350 g Sprague-Dawley rats were hand-picked and layered between acrylamide gel column beads (Bio-Gel P4G (156–4124)) in perifusion media (DMEM (Sigma, D5030)), supplemented with $NaHCO_3$, 10 mM HEPES, 4 mM glutamine, 0.2% fatty acid free BSA and 2.5 mM glucose). Eighty islets for each condition ($n = 4$) were perifused at a rate of 100 μl/min on an 8-channel BioRep Technologies perifusion device (Miami, FL). Islets were equilibrated on the instrument in basal (2.5 mM) glucose perifusion media for 45 min (and 48 h for extended treatment) prior to sample collection in a 5% CO_2/95% air, 37 °C constant environment. After the stabilization period, perifusate was collected for basal insulin secretion with rCela2a (2 μg/ml) versus vehicle control (glycerol/Tris PH v/v) followed by stimulatory glucose (9 mM) with or without rCela2a. Mouse rCela2a endotoxin levels were < 1.0 EU per 1 μg of the protein by the LAL method, using ToxinEraserTM Endotoxin Removal Kit, GeneScript, L00338, which is a standard level. Rat insulin was measured in the perfusate using a high range rat insulin ELISA (ALPCO) and normalized to total islet DNA concentration using Quant-it PicoGreen dsDNA Assay Kit (Life Technologies).

To test the effect of human CELA2A on rat islets, activated WT-CELA2A (1.5 μg/ml), activated p.D121N-CELA2A (1.5 μg/ml), vehicle control in activation buffer, or no treatment were applied as the same aforementioned protocol.

Insulin secretion of human islets.

Human islets from normal donors were purchased from Prodo Laboratories Inc. and were cultured immediately upon arrival in CMRL complete media consisting of glutamine free CMRL supplemented with 10 mM niacinamide and 16.7 μM zinc sulfate (Sigma), 1% ITS supplement (Corning), 5 mM sodium pyruvate, 1% Glutamax, 25 mM HEPES (American Bio), 10% HI FBS and antibiotics (10,000 units/ml penicillin and 10 mg/ml streptomycin). All media components were obtained from Life Technologies unless otherwise indicated. Human donor islets were cultured for 48 h at 37 °C 5% CO_2/95% prior to the insulin study.

Glucose stimulated insulin secretion in human islets was performed by perifusion in a similar fashion as the rat islets with the only differences being that 40 islets size matched by microscopy were picked for each condition (n = 4) at rate of 100 μl/min on a 12-channel BioRep Technologies perifusion device (Miami, FL). After the stabilization period, perifusate was collected for basal insulin secretion (2.5 mM glucose) followed by 2.5 mM glucose with vehicle control, WT-CELA2A, p.D121N-CELA2A, or no treatment which remained throughout the duration of the perifusion. After the basal period (20 min), the islets were stimulated with 9 mM glucose and samples were collected for 45 min to capture first and second phase insulin release. Human insulin was measured in the perfusate using a human insulin ELISA (ALPCO) and normalized to total islet DNA concentration using Quant-it PicoGreen dsDNA Assay Kit (Life Technologies).

Insulin signaling in 3T3L1 cells.

3T3L1 cells were starved for 24 h and subsequently treated with the WT-CELA2A (1.5 μg/ml), p.D121N-CELA2A (1.5 μg/ml), insulin (10 nM), and insulin (10 nM) pre-incubated insulin with WT- or p.D121N-CELA2A (1.5 μg/ml) for 4 h. Cells were harvested at the indicated time points (0, 15, 30, 45 min). Cell lysates were processed as described[42] and applied to 4–20% or 4–15% gradient SDS-PAGE. Immunoblotting was carried using target primary antibodies followed by appropriate HRP-conjugated secondary antibodies. Enhanced chemiluminescence reagents were applied to develop the blots, and blots were quantified with Bio-Rad Image Lab.

Imaging of intracellular Ca^{2+} transients.

Rat-derived clonal insulin 1 (INS-1) cells were plated on 22 × 22 mm glass coverslips 24 h prior to imaging. Cells were loaded with Fluo-4AM (6 μM, 30 min at 37 °C, ThermoFisher Scientific) in low glucose (2.5 mM) media and then washed two times with low glucose imaging buffer consisting of 130 mM NaCl, 5 mM KCl, 1 mM $MgSO_4$, 1.2 mM KH_2PO_4, 19.7 mM HEPES, 1.25 mM $CaCl_2$, and 2.5 mM or 9 mM dextrose. Cells were transferred to a custom-built perfusion chamber and imaged on a Zeiss LSM 710 DUO confocal microscope with a 40× objective. Different dextrose concentrations (2.5 mM and 9 mM) accompanied with Control Vehicle in activation buffer, activated WT-Cela2a (1.5 μg/ml), activated p.D121N-Cela2a (1.5 μg/ml) or no treatment were applied to the cells as indicated in individual graphs. Excitation was provided by a 488-nm laser and emission was collected above 505 nm. Images were collected at 0.2 Hz and analyzed post-acquisition on Image J software (National Institutes of Health). Fluorescence data is expressed as percentage of baseline over time according to the following equation: F/F_0*100 where F is the individual fluorescence at any given time; F_0 is the baseline fluorescence based on an average of the 5 initial fluorescence values for each cell. Each tracing corresponds to an individual cell. Area under the curve (AUC), which estimates total cytosolic Ca^{2+} release, was calculated in Prism 7 (GraphPad Software,).

Phosphoproteomics and gene set enrichment analysis of phosphorylation sites.

INS-1 cells were treated with rCela2a (2 μg/ml). Proteomic samples underwent in-gel tryptic digestion (V51111; Promega) and were subjected to information-dependent and SWATH acquisition, as described[43]. The latter was used for precursor ion quantification by Skyline

(v2.4) for the various phosphorylation sites. The degree phosphorylation at each site was used by the method described by Baucum et al. Other modifications, including cysteine carboxamido-methylation, methionine oxidation, were identified through the spectral library created in Skyline. Manual inspection was employed to verify modifications of the raw MS/MS fragmentation mass spectra for every assigned precursor mass containing the phosphorylation site. The areas under the isotopic envelope were calculated for M, M + 1, and M + 2 isotopic peaks for all variants of each phosphorylated peptide for each sample and the ratio of phosphorylated to total protein (phosphorylated + non-phosphorylated) was calculated for the M, M + 1, and M + 2 ions for each sample. The data are expressed as the ratio of phosphorylated/total recovered peptide and statistical analyses were performed using a one-way ANOVA (SigmaPlot), and significantly altered phosphorylated peptides ($P < 10^{-5}$) were used as an input for gene set enriched analysis using GO Enrichment Analysis. GO terms shared by the input genes are compared to the background distribution of the list annotated to that term. *P*-value is the probability for *n* number of input genes to the total number of annotated genes in any given GO term, based on the proportion of genes in the whole genome that are annotated to that GO term. Pathways are ranked based on fold enrichment for pathways with adjusted $P < 0.05$.

Isolation and preparation of human platelet suspension.

Venous blood was drawn from healthy adult volunteers ($n \geq 3$) who had taken no medications for at least two weeks. Platelet-rich plasma (PRP) was prepared from blood freshly drawn into citrate tubes by centrifugation at 250 RCF for 12 min at 25 °C. The platelet count in PRP was adjusted, if required, to 2–3 × 10^8/ml by the platelet-poor plasma of the same individual. The PRP was incubated at 37 °C for 90 min with purified WT- and p.D121N-CELA2A proteins at the final concentration of 1.5 μg/ml. The PRP tubes were either used for aggregation assay or for preparing washed platelets. Washed platelets were prepared by centrifugation of PRP at 700 RCF for 8 min. To avoid activation due to processing, PGI2 (20 ng/ml) was added to the PRP just before spinning it for washed platelet preparation. The platelet pellet was resuspended in a calcium free washing buffer (100 mM NaCl, 5 mM KCl, 1 mM $MgCl_2$, 5 mM glucose, 36 mM citric acid, 0.35% BSA, pH 6.5). These washed platelets were used either for flow cytometer-based assays or for imaging by confocal microscopy.

Platelet aggregation assay.

Platelet aggregation was performed on a dual channel Lumi-aggregometer (Model 700, Chrono-log) by optical method as per manufacturer's instructions. Platelet aggregation was recorded as percent increase in light transmission after adding collagen (Chrono-log) in human PRP at final concentration of 2 μg/ml with constant stirring (1,100 RPM). The channels were tested for confirming identical functioning to avoid any variations due to variation in channel performance. The maximum amplitude or maxA was used for recording the aggregation data and aggregation curves were merged using AGGRO/LINK8 software (Chrono-log).

Platelet surface activation and apoptosis assay (mitochondrial transmembrane potential loss (ΔΨm).

The PAC1 assay was used to analyze activation of GP2B3A receptor on platelet surface as described[44]. This assay uses an antibody that binds specifically to activated conformation of human GP2B3A receptor and not to its resting form[44]. The pretreated washed platelets were used for this assay. The FITC conjugated PAC1 antibody (340507, BD Biosciences) was added to washed platelets and after 20 min incubation before acquiring the events on flow cytometer. For apoptosis assay, the pretreated washed platelets were incubated with 1 μM tetramethylrhodamine methyl ester (TMRE) reagent (T669, Thermo Fisher Scientific) at 37 °C for 15 min followed by staining with annexin-V for 15 min in apoptosis assay buffer, as described[45]. This assay quantifies the cells with depolarized mitochondrial membrane and exposed phosphatidyl serine on the platelet surface. For both the assays, 3×10^4 events were acquired using special order BD LSR II Cell Analyzer (BD Biosciences) and data were analyzed by FlowJo v10 (FlowJo LLC).

Oral glucose tolerance test and hyperglycemic clamp.

Participants arrived at the Yale New Haven Hospital Research Unit in the morning of the study after at least an 8 h overnight fast. Baseline measurements of BMI and vital signs (BP, HR, RR) were measured. Females were assessed for pregnancy with a urine hCG test. After obtaining baseline hormone and glucose levels, subjects ingested 7.5 oz of glucola, which contains 75 g of glucose in orange flavored water. Blood samples were taken at −15, 0, 10, 20, 30, 60, 90, and 120 min for the measurement of plasma glucose. Insulin and glucagon levels were measured 60 and 120 min after ingesting glucola.

The same participants returned to the Hospital Research Unit for the hyperglycemic-clamp visit. An intravenous (IV) catheter was placed in the antecubital vein in each arm (one for glucose and insulin infusion and the other for blood draws). A baseline blood measure was done for glucose and hormone measurements: insulin, glucagon. Blood draws were drawn for glucose every 5–10 min. Insulin and glucagon were measured at baseline; and after 30 and 60 min after starting the bolus-continuous infusion of IV 20% dextrose solution. Dextrose solution was given at a variable infusion rate using an Alaris® pump to maintain glucose serum level ~200 mg/dL until the end of the hyperglycemic-clamp.

Statistical analyses.

In vivo studies included at least five mice in each group. *In vitro* studies were carried out in more than 3 independent experiments. Preparation of graphs and all statistical analyses, including 2-tailed Student *t*-test, 1-way ANOVA (SigmaPlot)) and testing for equal variance were carried out using GraphPad Prism 8.1 Project software (GraphPad Software Inc.). Fisher's exact test was carried out for the continuous variables. $P < 0.05$ was considered significant. Data are presented as mean ± s.e.m. Fluorescence Images were evaluated by Image J software (National Institutes of Health).

Reporting Summary.

Further information on study design is available in the Nature Research Reporting Summary linked to this article.

Data availability.

Human variants and phenotypes have been reported to ClinVar under accession numbers SCV000916382, SCV000916383, SCV000916384, and SCV000916385. The data are also reported to NIH with other identified variants in the Yale Center for Mendelian Genomics. Proteomics data are available upon request.

Supplementary Material

Refer to Web version on PubMed Central for supplementary material.

Acknowledgements

We thank Tukiet Lam, Jean Kanyo, Weiwei Wang, and Navin Rauniar from Yale Keck MS & Proteomic Services for their help with the proteomics analysis, and James Murphy from Yale Department of Pharmacology for preparing the ribbon diagrams. This work was supported by grants from the National Institutes of Health (NIH) (RHL135767A), and P30 DK34989 to A.M., NIH R01DK095753 to M.S.-T., NIH T32DK grant to F.E. (DK007356), a grant from the NIH Centers for Mendelian Genomics (5U54HG006504) and a VA Merit Award to F.G. NIH S10 (SIG) OD018034 awarded to the Mass Spectrometry (MS) & Proteomics Resource of the W.M. Keck Foundation Biotechnology Resource Laboratory at Yale University.

References

1. Murray CL and Lopez AD Global mortality, disability, and the contribution of risk factors: Global Burden of Disease Study. Lancet 349, 1436–1442 (1997). [PubMed: 9164317]
2. Malik S et al. Impact of the metabolic syndrome on mortality from coronary heart disease, cardiovascular disease, and all causes in United States adults. Circulation 110, 1245–1250 (2004). [PubMed: 15326067]
3. Marenberg M, Risch N, Berkman LF, Floderus B and Defaire U Genetic susceptibility to death from coronary heart-disease in a study of twins. N. Engl. J. Med 330, 1041–1046 (1994). [PubMed: 8127331]
4. Abifadel M et al. Mutations in PCSK9 cause autosomal dominant hypercholesterolemia. Nat. Genet 34, 154–156 (2003). [PubMed: 12730697]
5. Mani A et al. LRP6 mutation in a family with early coronary disease and metabolic risk factors. Science 315, 1278–1282 (2007). [PubMed: 17332414]
6. Keramati AR et al. A form of the metabolic syndrome associated with mutations in DYRK1B. N. Engl. J. Med 370, 1909–1919 (2014). [PubMed: 24827035]
7. Szepessy E & Sahin-Toth M Inactivity of recombinant ELA2B provides a new example of evolutionary elastase silencing in humans. Pancreatology 6, 117–122 (2006). [PubMed: 16327289]
8. Largman C, Brodrick JW & Geokas MC Purification and characterization of two human pancreatic elastases. Biochemistry 15, 2491–2500 (1976). [PubMed: 819031]
9. Adzhubei IA et al. A method and server for predicting damaging missense mutations. Nat. Methods 7, 248–249 (2010). [PubMed: 20354512]
10. Warren HR et al. Genome-wide association analysis identifies novel blood pressure loci and offers biological insights into cardiovascular risk. Nat. Genet 49, 403–415 (2017). [PubMed: 28135244]
11. Wain LV et al. Novel blood pressure locus and gene discovery using genome-wide association study and expression data sets from blood and the kidney. Hypertension doi: 10.1161/HYPERTENSIONAHA.117.09438 (2017).
12. Hoffmann TJ et al. Genome-wide association analyses using electronic health records identify new loci influencing blood pressure variation. Nat. Genet 49, 54–64 (2017). [PubMed: 27841878]
13. Fersht A and Sperling J The charge relay system in chymotrypsin and chymotrypsinogen. J. Mol. Biol 74, 137–149 (1973). [PubMed: 4689953]
14. Frey PA, Whitt SA & Tobin JB A low-barrier hydrogen bond in the catalytic triad of serine proteases. Science 264, 1927–1930 (1994). [PubMed: 7661899]

15. Oleksyszyn J & Powers JC Irreversible inhibition of serine proteases by peptide derivatives of (alpha-aminoalkyl)phosphonate diphenyl esters. Biochemistry 30, 485–493 (1991). [PubMed: 1988040]
16. Sprang S et al. The three-dimensional structure of Asn102 mutant of trypsin: role of Asp102 in serine protease catalysis. Science 237, 905–909 (1987). [PubMed: 3112942]
17. Yang X, Pratley RE, Tokraks S, Bogardus C & Permana PA Microarray profiling of skeletal muscle tissues from equally obese, non-diabetic insulin-sensitive and insulin-resistant Pima Indians. Diabetologia 45, 1584–1593 (2002). [PubMed: 12436343]
18. Marselli L et al. Gene expression profiles of Beta-cell enriched tissue obtained by laser capture microdissection from subjects with type 2 diabetes. PLoS One 5, e11499 (2010). [PubMed: 20644627]
19. Hulme JT et al. Sites of proteolytic processing and noncovalent association of the distal C-terminal domain of CaV1.1 channels in skeletal muscle. Proc. Natl. Acad. Sci. USA 102, 5274–5279 (2005). [PubMed: 15793008]
20. Gao T et al. C-terminal fragments of the alpha 1C (CaV1.2) subunit associate with and regulate L-type calcium channels containing C-terminal-truncated alpha 1C subunits. J. Biol. Chem 276, 21089–21097 (2001). [PubMed: 11274161]
21. Daly C & Ziff EB Post-transcriptional regulation of synaptic vesicle protein expression and the developmental control of synaptic vesicle formation. J. Neurosci 17, 2365–2375 (1997). [PubMed: 9065497]
22. Liu G, Hilliard N & Hockerman GH Cav1.3 is preferentially coupled to glucose-induced [Ca2+]i oscillations in the pancreatic beta cell line INS-1. Mol. Pharmacol 65, 1269–1277 (2004). [PubMed: 15102955]
23. Steneberg P et al. The type 2 diabetes-associated gene ide is required for insulin secretion and suppression of alpha-synuclein levels in beta-cells. Diabetes 62, 2004–2014 (2013). [PubMed: 23349488]
24. Farris W et al. Insulin-degrading enzyme regulates the levels of insulin, amyloid beta-protein, and the beta-amyloid precursor protein intracellular domain in vivo. Proc. Natl. Acad. Sci. USA 100, 4162–4167 (2003). [PubMed: 12634421]
25. Schilling RJ & Mitra AK Degradation of insulin by trypsin and alpha-chymotrypsin. Pharm. Res 8, 721–727 (1991). [PubMed: 2062801]
26. Poy MN et al. CEACAM1 regulates insulin clearance in liver. Nat. Genet 30, 270–276 (2002). [PubMed: 11850617]
27. Shattil SJ, Hoxie JA, Cunningham M & Brass LF Changes in the platelet membrane glycoprotein IIb.IIIa complex during platelet activation. J. Biol. Chem 260, 11107–11114 (1985). [PubMed: 2411729]
28. Yeh JJ et al. P-selectin-dependent platelet aggregation and apoptosis may explain the decrease in platelet count during Helicobacter pylori infection. Blood 115, 4247–4253 (2010). [PubMed: 20097880]
29. Keinan A & Clark AG Recent explosive human population growth has resulted in an excess of rare genetic variants. Science 336, 740–743 (2012). [PubMed: 22582263]
30. Kato S et al. Increased calcium-channel currents of pancreatic beta cells in neonatally streptozocin-induced diabetic rats. Metabolism 43, 1395–1400 (1994). [PubMed: 7526124]
31. Calanna S et al. Secretion of glucagon-like peptide-1 in patients with type 2 diabetes mellitus: systematic review and meta-analyses of clinical studies. Diabetologia 56, 965–972 (2013). [PubMed: 23377698]
32. Herzberg-Schafer S, Heni M, Stefan N, Haring HU & Fritsche A Impairment of GLP1-induced insulin secretion: role of genetic background, insulin resistance and hyperglycaemia. Diabetes Obes. Metab 14 Suppl 3, 85–90 (2012). [PubMed: 22928568]
33. Pidard D, Frelinger AL, Bouillot C & Nurden AT Activation of the fibrinogen receptor on human platelets exposed to alpha chymotrypsin. Relationship with a major proteolytic cleavage at the carboxyterminus of the membrane glycoprotein IIb heavy chain. Eur. J. Biochem 200, 437–447 (1991). [PubMed: 1889410]

34. Robert L, Jacob MP and Labat-Robert J Cell-matrix interactions in the genesis of arteriosclerosis and atheroma: effect of aging. Ann. NY Acad. Sci 673, 331–341 (1992). [PubMed: 1336648]

35. Katsunuma H, Shimizu K, Iwamoto T, and Kiyokawa M Anti-atherosclerotic action of elastase - with special reference to its effect on elastic fibres. Age and Ageing 12, 183–194 (1983). [PubMed: 6556003]

36. Zureik M, Robert L, Courbon D, Touboul PJ, Bizbiz L, and Ducimetiere P Serum elastase activity, serum elastase inhibitors, and occurrence of carotid atherosclerotic plaques: the Etude sur le Vieillissement Arteriel (EVA) Study. Circulation 205, 2638–2645 (2002).

37. Tzoulaki I et al. Relative value of inflammatory, hemostatic, and rheological factors for incident myocardial infarction and stroke: the Edinburgh Artery Study. Circulation 115, 2119–2127 (2007). [PubMed: 17404162]

38. Talukdar S et al. Neutrophils mediate insulin resistance in mice fed a high-fat diet through secreted elastase. Nat. Med 18, 1407–1412 (2012). [PubMed: 22863787]

Methods-only References

39. Lee J, Hong YP, Shin HJ & Lee W Associations of sarcopenia and sarcopenic obesity with metabolic syndrome considering both muscle mass and muscle strength. J. Prev. Med. Public Health 49, 35–44 (2016). [PubMed: 26841883]

40. Exome Variant Server, Seattle, WA (URL: http://evs.gs.washington.edu/EVS/) [June 2013 accessed].

41. Szabo A, Pilsak C, Bence M, Witt H & Sahin-Toth M Complex formation of human proelastases with procarboxypeptidases A1 and A2. J. Biol. Chem 291, 17706–17716 (2016). [PubMed: 27358403]

42. Go GW et al. The combined hyperlipidemia caused by impaired Wnt-LRP6 signaling is reversed by Wnt3a rescue. Cell Metab 19, 209–220 (2014). [PubMed: 24506864]

43. Miller MB et al. Brain region and isoform-specific phosphorylation alters kalirin SH2 domain interaction sites and calpain sensitivity. ACS Chem. Neurosci 8, 1554–1569 (2017). [PubMed: 28418645]

44. Shattil SJ, Hoxie JA, Cunningham M & Brass LF Changes in the platelet membrane glycoprotein IIb.IIIa complex during platelet activation. J. Biol. Chem 260, 11107–11114 (1985). [PubMed: 2411729]

45. Lee SH et al. Inducing mitophagy in diabetic platelets protects against severe oxidative stress. EMBO Mol. Med 8, 779–795 (2016). [PubMed: 27221050]

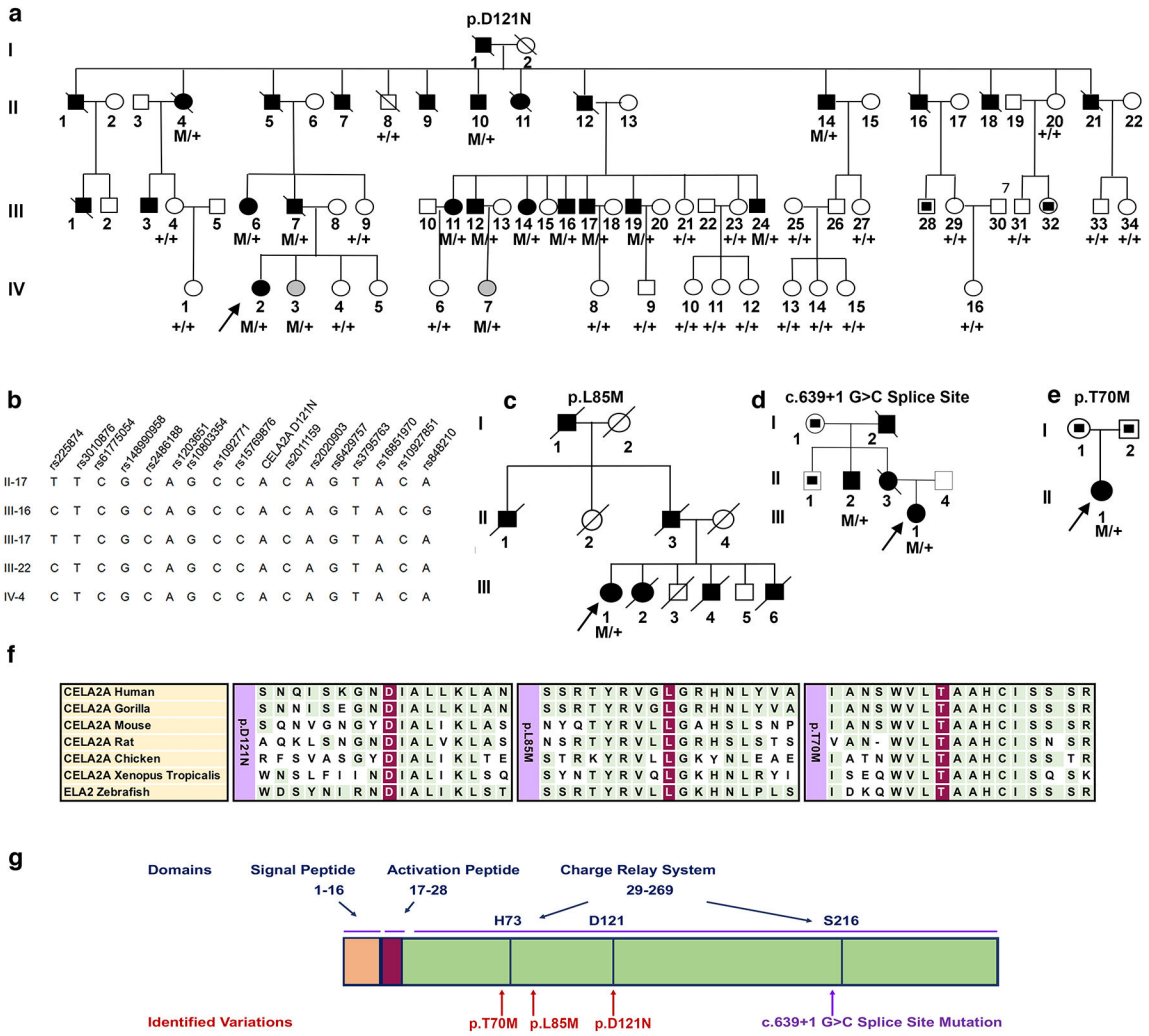

Fig. 1 |. Schematics showing CELA2A pedigrees, amino acid substitutions and conservation.

a, Pedigree structure of the kindred with the p.D121N substitution in CELA2A. **b**, Minimum shared haplotype in affected individuals. **c-e**, Kindreds with the CELA2A p.L85M substitution (**c**), splice site mutation (c.639+1 G>C) (**d**), and p.T70M substitution (**e**). The index cases are denoted with arrows. The CAD phenotype is indicated by symbols filled in black. Males are represented by squares, and females are represented by circles. Symbols that are struck through represent deceased individuals. Gray symbols represent subjects with metabolic traits, too young to develop CAD; dotted symbols represent subjects with unknown status. **f**, Amino acid sequences of the CELA2A region flanking Asp121, Leu85, and Thr70 showing their conservation in a variety of vertebrate species. **g**, Schematic representation of CELA2A protein primary structure depicting the locations of amino acid substitutions (red), and the splice site (purple) mutation in relation to different protein domains.

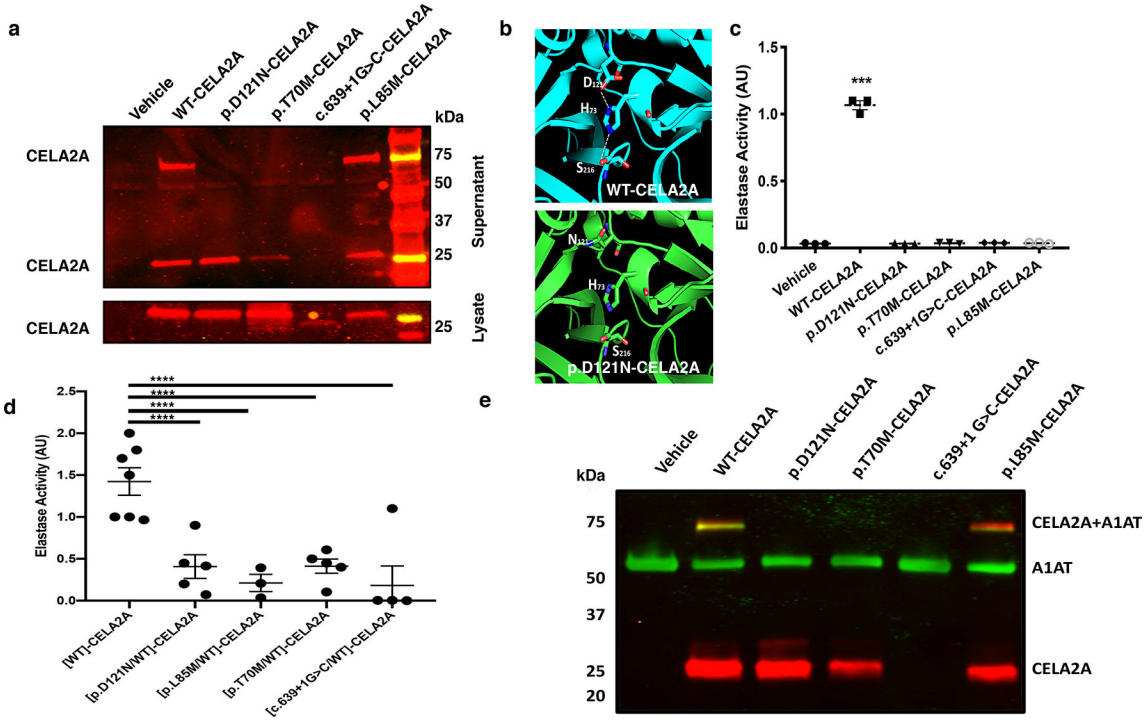

Fig. 2 |. Human wild-type and mutant CELA2A structures and functions.

a, Western blot image demonstrating His-WT-, His-p.D121N-, His-p.T70M-, His-c.639+1G>C- and His-p.L85M-CELA2A expressed in HEK293T cells from cell lysate (bottom panel) and secreted (supernatant, upper panel). An extra band at 75 kDa is present in secreted WT-CELA2A and p.L85M-CELA2A, verified as CELA2A protein by proteomic analysis ($n = 3$ replicated experiments). **b**, Ribbon diagram representations of the catalytic triad within the crystal structures of WT- and p.D121N-CELA2A are shown. In the upper panel, Asp121 and the hydrogen bonds between its beta-carboxyl group and N delta 1 of His73 are shown. The lower panel shows p.D121N substitution, which disrupts hydrogen bonds. **c**, In vitro elastase activity of purified WT and different mutant CELA2A proteins (mean ± s.e.m.; $n = 3$ replicated experiments, one-way ANOVA, 95% CI, ***$P = 0.001$). **d**, Dot plot demonstrating the elastase activity of WT-CELA2A coexpressed with different mutant CELA2A proteins (mean ± s.e.m; $n = 2$ replicated experiments, one-way ANOVA, 95%CI, ****$P < 0.0001$). **e**, Western blot analysis of A1AT (α1-antitrypsin), treated with WT-, p.D121N-, p.T70M-, c.639+1G>C- and p.L85M-CELA2A. Red color depicts CELA2A, green the A1A2 and yellow the merging of the two, indicating their complex formation. The 75-kDa band of WT- and p.L85M-CELA2A bound to A1AT are shown (lanes 2 and 6). The 75-kDa band is absent in all other mutant CELA2A proteins (lanes 3–5) ($n = 3$ replicated experiments). AU, arbitrary unit.

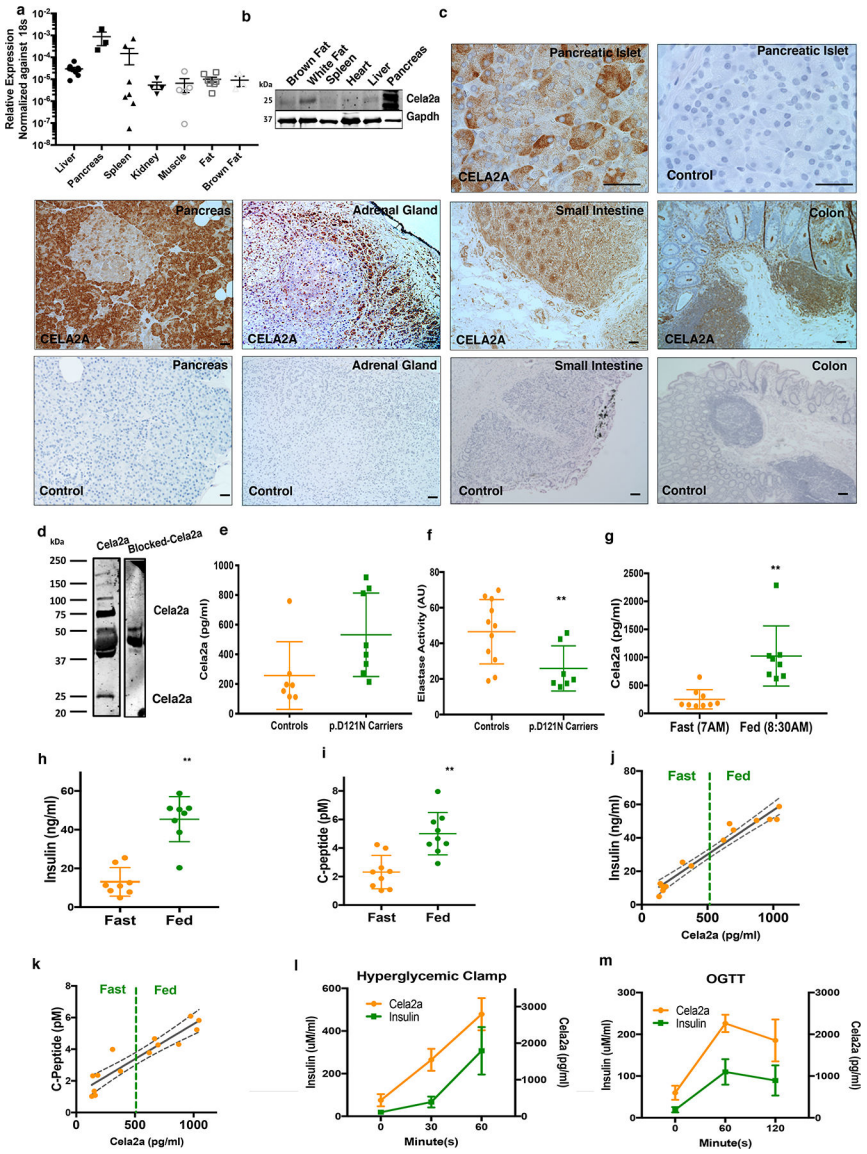

Fig. 3 |. Mouse and human Cela2a tissue expression, human CELA2A plasma levels and activities.

a,b, Cela2a mRNA (mean ± s.e.m.) and protein levels in different mouse tissues ($n = 6$ mice). **c**, Immunohistochemical staining of human tissues using CELA2A-specific antibody. The controls without primary antibodies are shown underneath ($n = 1$). **d**, Western blot analysis of CELA2A in human serum (75-kDa and 25-kDa Cela2a bands). Both bands are absent in the parallel western blot performed on human serum using CELA2A-specific antibody preblocked with rCela2a ($n = 2$ replicated experiments). Whole blot is shown in Supplementary Fig. 7. **e,f**, Total plasma CELA2A levels (**e**) and elastase activity (**f**) (mean ± s.e.m.) measured in p.D121N carriers vs. noncarriers measured by validated ELISA assay ($n = 7$ in each group, two-tailed Student's t-test, $^{**}P < 0.01$). **g-i**, Baseline and postprandial plasma CELA2A, insulin and c-peptide levels (mean ± s.e.m.; $n = 8$, two-tailed Student's t-test, $P = 0.0009$, $P < 0.0001$ and $P = 0.0006$, respectively). **j,k**, Correlation of baseline and postprandial plasma insulin and C-peptide with plasma CELA2A in random healthy subjects

presented as values ($n = 8$, age 20–30 y). Correlation coefficient for **j** and **k** was performed using GraphPad Prism8. **l,m**, Plasma glucose and CELA2A levels (mean ± s.e.m.) during hyperglycemic clamps and OGTT in obese nondiabetic subjects, respectively ($n = 5$). OGTT, oral glucose tolerance test; AU, arbitrary unit. Scale bar, 100 μm.

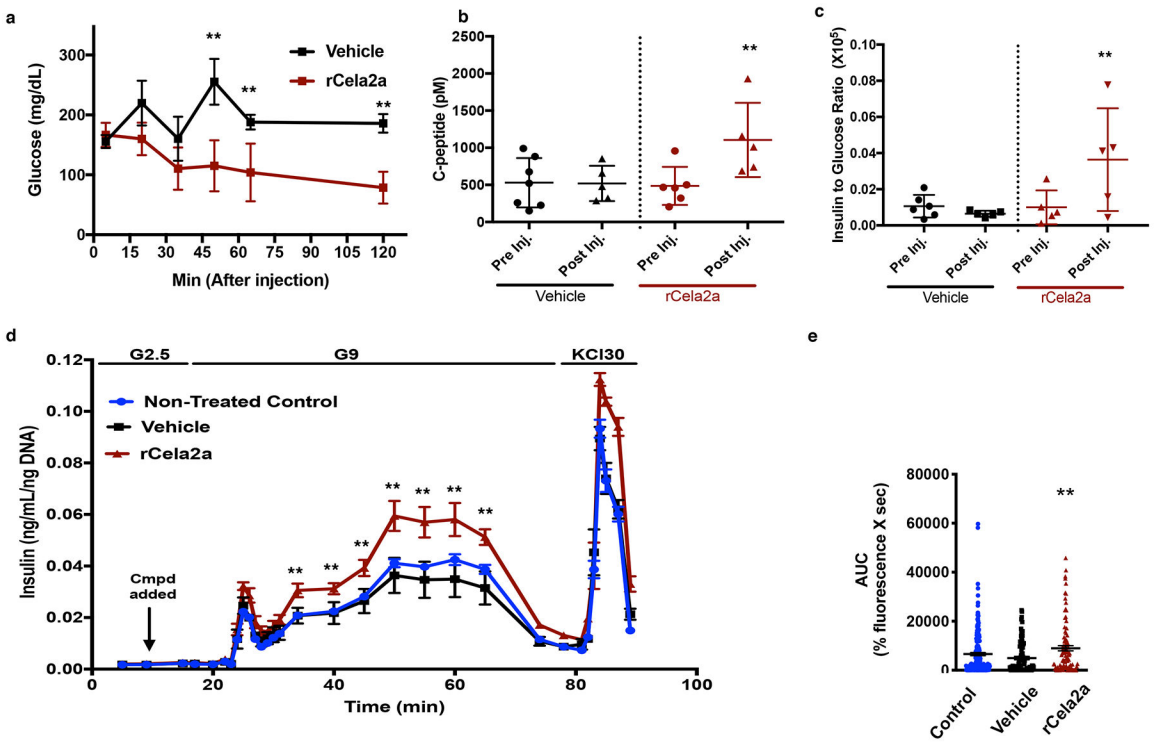

Fig. 4 |. Cela2a induction of insulin secretion in vivo and in vitro.

a-c, Plasma glucose (**a**), C-peptide (**b**) and insulin to glucose ratios (**c**) (mean ± s.e.m.) in hyperlipidemic and hyperglycemic Ldlr$^{-/-}$ mice injected with rCela2a (recombinant mouse Cela2a) or vehicle ($n = 5$ mice in each group in 2 replicated experiments, one-way ANOVA, $P < 0.01$, $P = 0.0096$, $P = 0.0196$). **d**, Insulin response (mean ± s.e.m.) of rat islets to rCela2a (50 nM) or vehicle at 2.5 mM and 9 mM glucose concentrations. KCl was used as a positive control and test of viability ($n = 3$ replicated experiments, two-tailed Student's t-test, $^{**}P < 0.01$). **e**, Area under the curve (AUC) of Ca^{2+} transient (mean ± s.e.m.) upon treatment of INS-1 cells with rCela2a, demonstrating greater calcium transient in rCela2a-treated cells compared to 9 mM glucose medium served as a control or vehicle-treated cells ($n = 3$ replicated experiments, two-tailed Student's t-test, $^{**}P = 0.0045$).

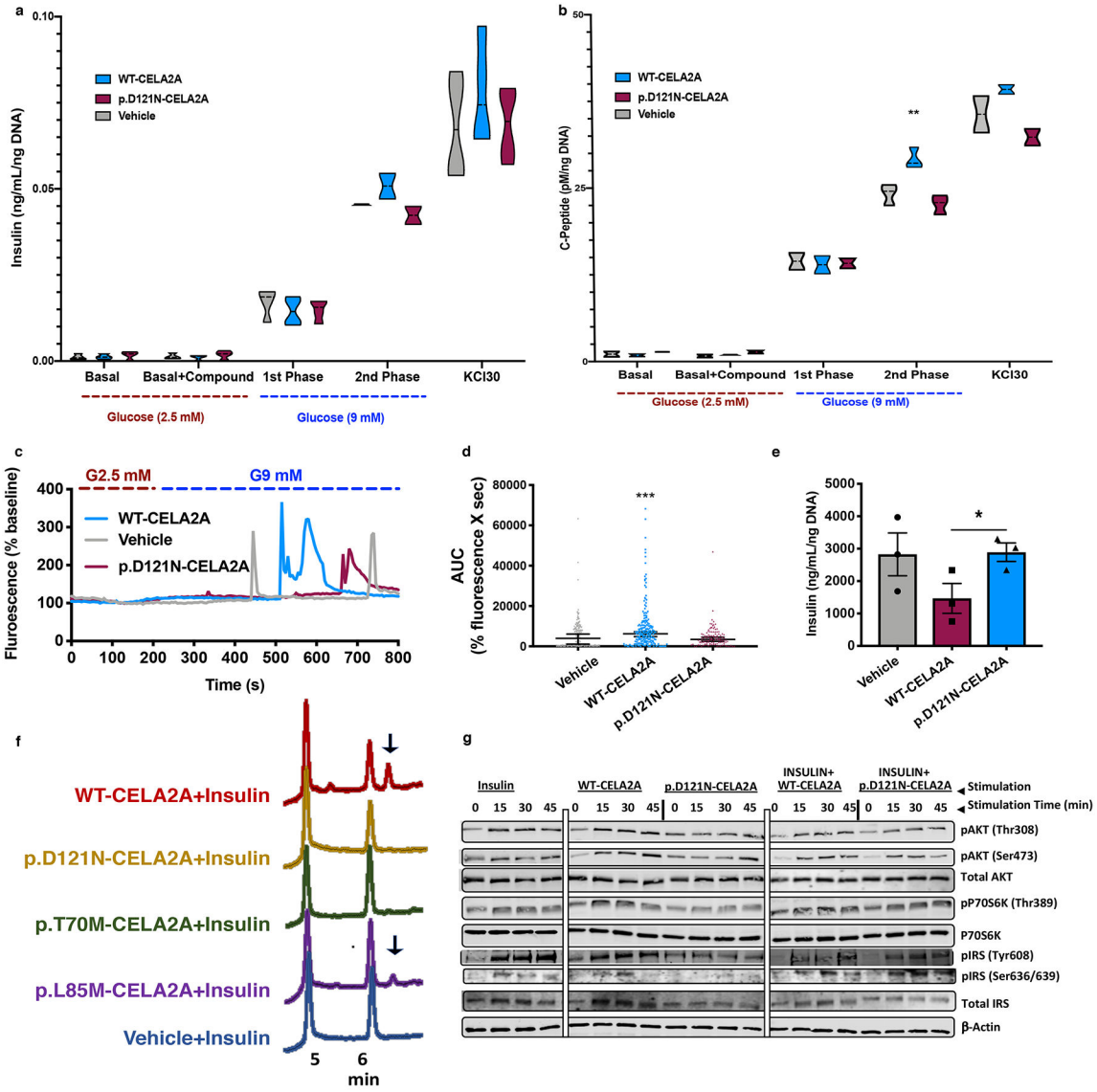

Fig. 5 |. Insulin secretion, degradation and sensitivity of WT-CELA2A and p.D121N-CELA2A proteins.

a,b, Insulin (**a**) and C-peptide (**b**) secretion of rat islets in response to WT-CELA2A (50 nM), p.D121N-CELA2a or vehicle at 2.5 mM and 9 mM glucose concentrations represented as violin plots demonstrating mean, minimum and maximum ($n = 4$, in two replicated experiments, $^{**}P < 0.01$). KCl was used as a positive control and test of viability. **c,d**, Representative of calcium transient upon treatment of INS-1 cells with WT- vs. p.D121N-CELA2A and area under the curve (AUC) of Ca^{2+} transient, represented as dot plots (mean ± s.e.m.; $n = 3$ biologically independent experiments demonstrating greater calcium transient in WT-CELA2A treated cells; statistical comparisons were performed using one-way ANOVA, 95%CI, $^{***}P < 0.0001$). **e**, Insulin content (mean ± s.e.m) in the media of rat islets treated with WT- and p.D121N-CELA2A for 48 h represented as dot plots; $n = 3$ replicated experiments, statistical comparisons were performed using two-sided Student's *t*-test, 90% CI, $P < 0.05$). **f**, UPLC analysis of insulin digestion by WT-, p.D121N-, p.T70M-, and

p.L85M-CELA2A ($n = 2$ replicated experiments). Arrows show fragmented insulin. **g**, Western blot analysis of insulin/mTOR signaling pathways in 3T3L1 cells treated with insulin, WT- or p.D121N-CELA2A, and predigested insulin with WT- or p.D121N-CELA2A CELA2A ($n = 2$ biologically independent experiments; quantification in Supplementary Fig. 6, whole blot in Supplementary Fig. 7).

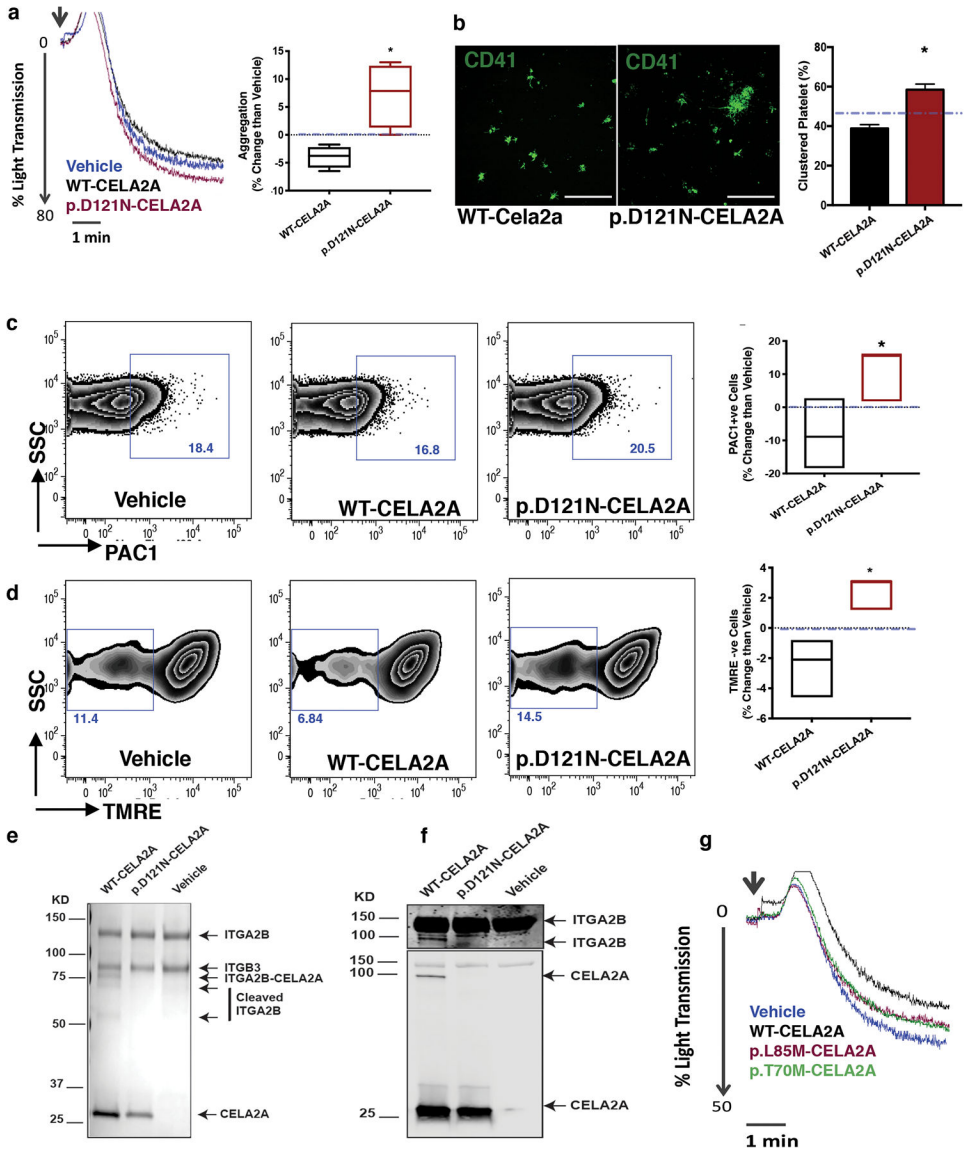

Fig. 6 |. Effect of WT- vs. p.D121N-CELA2A on platelet activity compared to the vehicle.

a, Representative tracings and percent platelet aggregation after incubating the platelet of healthy individuals with WT- or p.D121N-CELA2A relative to non-treated control, shown as box and whisker plots, demonstrating median, minimum and maximum ($n = 4$ replicated experiments, statistical comparisons performed using one-way ANOVA, 95% CI, $P = 0.041$). Vehicle is shown as dashed line. **b**, Platelet micrographs showing confocal images of CD41 stained platelets treated with either WT- or p.D121N-CELA2A. The percent platelet aggregation compared to untreated control shown in the adjacent bar charts graphs with mean ± s.e.m. ($n = 3$ biologically independent experiments). The statistical comparisons were performed using one-way ANOVA, 95% CI, $*P < 0.05$. Vehicle is shown as dashed line. **c**, Flowcytometry plots of FITC-PAC1 stained platelets treated with Vehicle, WT- and p.D121N-CELA2A (%PAC1-positive are shown within smaller boxes). The percent PAC1-positive platelets normalized against vehicle (dashed line) are represented as box and

whisker plots, demonstrating median, minimum and maximum in the adjacent graph ($n = 3$ biologically independent experiments), statistical comparisons were performed using one-way ANOVA, 95% CI, $*P = 0.049$). **d**, Flowcytometry plots of TMRE-stained platelets treated with vehicle, WT- and p.D121N-CELA2A (%TMRE-negartive fractions are shown inside the gates). The percent TMRE-negative platelets normalized against vehicle represented as box and whisker plots, demonstrating median, minimum and maximum are shown in the adjacent graph ($n = 3$ biologically independent experiments). The statistical comparisons were performed using one-way ANOVA; 95% CI,$*P = 0.016$, blue dashed line represents vehicle. **e**, Coomassie blue of GPIIb/IIIa treated either with vehicle, WT- or p.D121N-CELA2A. The identity of proteins shown for each band was verified by proteomics analysis ($n = 3$ replicated experiments). **f**, Western blot analysis of GPIIb/IIIa treated with vehicle, WT- or p.D121N-CELA2A using anti-ITGA2B (top) and anti-Cela2a antibodies (bottom) ($n = 3$ replicated experiments). **g**, Representative aggregation tracings of WT-, p.L85M-, p.T70M-CELA2A compared to vehicle ($n = 3$ replicated experiments).

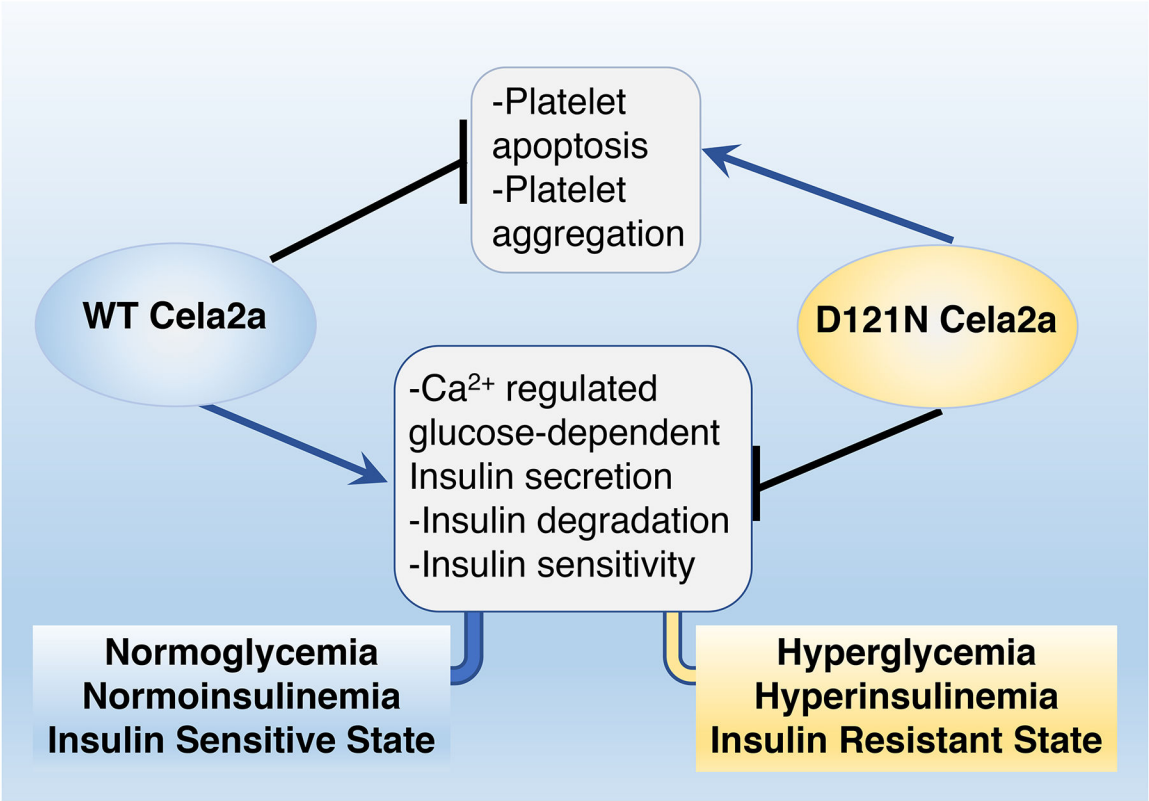

Fig. 7 |.
Schematic of CELA2A actions and its malfunction in p.D121N-CELA2A.